

Solitons in a trapped spin-1 atomic condensate

Wenxian Zhang,^{1,3} Ö. E. Müstecaplıoğlu,² and L. You³

¹*Ames Laboratory, Iowa State University, Ames, Iowa 50011, USA*

²*Department of Physics, Koç University, Sarıyer, İstanbul, 34450, Turkey, and*

³*School of Physics, Georgia Institute of Technology, Atlanta, Georgia 30332, USA*

(Dated: December 2, 2024)

We numerically investigate a particular type of spin solitons inside a trapped atomic spin-1 Bose-Einstein condensate (BEC) with ferromagnetic interactions. Within the mean field theory approximation, our study of the solitonic dynamics shows that the solitonic wave function, its center of mass motion, and the local spin evolutions are stable and are intimately related to the domain structures studied recently in spin-1 ^{87}Rb condensates. We discuss a rotating reference frame wherein the dynamics of the solitonic local spatial spin distribution become time independent.

PACS numbers: 03.75.Mn, 03.75.Lm, 03.75.Kk, 89.75.Kd

I. INTRODUCTION

Solitonic structure is an interesting and common subject in nonlinear science. It has been extensively studied in nonlinear optics [1], fluids [2] and plasmas [3], magnetic films [4], nanotubes [5], and recently in quantum superfluid of atomic Bose-Einstein condensates [6]. In nontechnical terms, the shape of a soliton remains unaltered during propagation due to a balance of the spreading from its dispersion with nonlinear interactions. This feature has been applied with great success in optical soliton based advanced communications.

As realized in recent years an atomic Bose-Einstein condensate (BEC) provides a new and powerful tool for the study of nonlinear phenomena. At weak interactions, a condensate is successfully modelled by the Gross-Pitaevskii (GP) equation, or the nonlinear Schrödinger equation (NLSE) [7, 8, 9, 10, 11, 12]. Feshbach resonance in recent years has provided a practical mechanism for adjusting the atomic s-wave scattering length through which both the sign and the strength of the atomic interactions become adjustable [13]. Bright matter wave soliton trains were realized in a ^7Li condensate due to its attractive atom-atom interaction, while gray and dark solitons were realized for repulsively interacting condensates through the phase engineering technique on the condensate wave function [14, 15].

Solitons with more than one parameter are often referred to as vector solitons. For instance, vector solitons are created in nonlinear optics if different polarizations or spatial modes of light in an optical fiber are taken as parameters. This could easily be implemented in a spinor condensate as the atomic internal degrees of freedom become available. Many have suggested creating a Manakov soliton in a two-component BEC with attractive self-interactions [16]. Symbiotic solitons have also been investigated in a two-component BEC with repulsive self-interactions accompanied by attractive cross-interactions [17]. Domain wall solitons can be created in a trapped two-component condensate even when both self- and cross-interactions are repulsive [18].

With a far off resonant optical trap, all hyperfine states

of an atom can be confined simultaneously, thus realizing a spinor condensate, as has been reported in many experiments with ^{23}Na and ^{87}Rb atoms [19, 20, 21, 22, 23, 24, 25, 26, 27]. The releasing of the spin degree of freedom has led to many novel properties lacking in a single component or scalar condensate. For instance, the spin exchange interaction as in a spin-1 condensate, whereby two $|F = 1, m_F = 0\rangle$ atoms are converted into one $|F = 1, m_F = +1\rangle$ atom, and one $|F = 1, m_F = -1\rangle$ atom upon an elastic collision, already well understood [28, 29, 30], also helps to support the existence of spinor solitons. In a homogeneous system, exact soliton solutions for an attractively interacting spin-1 condensate have been recently obtained analytically [31]. Also theoretical investigations have been carried out on magnetic (or spinor) solitons in a ferromagnetically interacting spin-1 condensate [32, 33].

In this paper, we focus on the more realistic case of spin solitons inside trapped atomic condensates (of ^{87}Rb). First we attempt to numerically find solitonic structures through the propagation in time of the GP equation for a trapped spin-1 condensate. Then we demonstrate that the dynamics of the found spin solitons is stable and is related to the multi-domain structure as studied recently [34, 35]. Finally, we discuss a rotating reference frame wherein the local spin distribution of the spinor condensate becomes stationary like a spatially propagating soliton in a moving reference frame.

This paper is organized as follows. In Sec. I we give an introduction and discuss the motivations for our work. The theoretical formulation is based on a model system of a spin-1 condensate as is presented in Sec. II. Section III describes the numerically obtained soliton state, while Sec. IV focuses on the investigation of the solitonic state's dynamics, center of the mass motion, and local spin distribution. In Sec. V we discuss a rotating reference frame and show that the local spin distribution becomes time-independent within this frame. Finally we conclude in Sec. VI.

II. REVIEW OF AN EFFECTIVE QUASI-ONE-DIMENSIONAL DESCRIPTION

A gas of interacting spin-1 atoms is described by the following second quantized Hamiltonian (summation over repeated indices is assumed) [28, 29, 30]

$$H = \int d\vec{r} \left[\Psi_i^\dagger \left(-\frac{\hbar^2}{2M} \nabla^2 + V_{\text{ext}}(\vec{r}) \right) \Psi_i + \frac{c_0}{2} \Psi_i^\dagger \Psi_j^\dagger \Psi_j \Psi_i + \frac{c_2}{2} \Psi_k^\dagger \Psi_i^\dagger (F_\gamma)_{ij} (F_\gamma)_{kl} \Psi_j \Psi_l \right], \quad (1)$$

where $\Psi_j(\vec{r})$ (Ψ_j^\dagger) is the field operator that annihilates (creates) an atom in the j th internal state at location \vec{r} , $j = +, 0, -$ denotes atomic hyperfine state $|F = 1, m_F = +1, 0, -1\rangle$, respectively. M is the mass of each atom, and $V_{\text{ext}}(\vec{r})$ is an internal state independent trap potential. Terms with coefficients c_0 and c_2 of Eq. (1) describe elastic collisions of two spin-1 atoms expressed in terms of the scattering lengths a_0 (a_2) in the combined symmetric channel of total spin 0 (2), $c_0 = 4\pi\hbar^2(a_0 + 2a_2)/3M$, and $c_2 = 4\pi\hbar^2(a_2 - a_0)/3M$. $F_{\gamma=x,y,z}$ are spin-1 matrices.

The equation of motion for the field operator in the Heisenberg picture is given by

$$i\hbar \frac{\partial}{\partial t} \Psi_i(\vec{r}, t) = [\Psi_i, H]. \quad (2)$$

Adopting a mean field theory approach by assuming that the condensate consists of a large number of atoms, we introduce the condensate order parameter or wave function $\Phi_i = \langle \Psi_i \rangle$ for the i th component. Neglecting quantum fluctuations we arrive at the coupled Gross-Pitaevskii equations

$$\begin{aligned} i\hbar \frac{\partial}{\partial t} \Phi_+ &= [\mathcal{L} + c_2(n_+ + n_0 - n_-)] \Phi_+ + c_2 \Phi_0^2 \Phi_-^*, \\ i\hbar \frac{\partial}{\partial t} \Phi_0 &= [\mathcal{L} + c_2(n_+ + n_-)] \Phi_0 + 2c_2 \Phi_+ \Phi_- \Phi_0^*, \\ i\hbar \frac{\partial}{\partial t} \Phi_- &= [\mathcal{L} + c_2(n_- + n_0 - n_+)] \Phi_- + c_2 \Phi_0^2 \Phi_+^*, \end{aligned} \quad (3)$$

where $\mathcal{L} = -(\hbar^2/2M) \nabla^2 + V_{\text{ext}}(\vec{r}) + c_0 n$, $n = \sum_i n_i$ is the total condensate density, and $n_i = |\Phi_i|^2$. Another way to derive the above coupled GP Eqs. (3) is to take the variations of the energy functional with respect to the condensate wave function

$$i\hbar \frac{\partial}{\partial t} \Phi_i = \frac{\delta E[\Phi_i, \Phi_i^*]}{\delta \Phi_i^*},$$

where

$$\begin{aligned} E[\Phi_i, \Phi_i^*] &= \int d\vec{r} \left[\Phi_i^* \left(-\frac{\hbar^2}{2M} \nabla^2 + V_{\text{ext}} + \frac{1}{2} c_0 n \right) \Phi_i \right. \\ &\quad \left. + \frac{1}{2} c_2 \Phi_k^* \Phi_i^* (F_\gamma)_{ij} (F_\gamma)_{kl} \Phi_j \Phi_l \right]. \end{aligned} \quad (4)$$

Inside a trap with tight radial confinement, the condensate assumes a prolate shape. Several effective one-dimensional (1D) approaches have already been developed [36, 37, 38, 39, 40, 41], with the simplest of

them assuming a fixed transverse Gaussian profile. Recent studies, however, have indicated that the effective quasi-1D non-polynomial Schrödinger equation (NPSE) is the more appropriate choice. In fact for most systems of interest, NPSE represents the most powerful and efficient tool especially in the weakly interacting limit [36, 37, 38, 41]. In several recent experiments, a single running wave optical trap is used to confine spin-1 atomic condensates, a situation well described by the quasi-one-dimensional trapping geometry [23, 24, 25, 26]. More precisely the external cigar-shaped trap is described by a harmonic trap potential $V_{\text{ext}} = (M/2)(\omega_\perp^2 r_\perp^2 + \omega_z^2 z^2)$ with $\omega_x = \omega_y = \omega_\perp$, $r_\perp = \sqrt{x^2 + y^2}$, and $\omega_z \ll \omega_\perp$. The quasi-one-dimensional NPSE description assumes a factorized wave function

$$\Phi_i(\vec{r}_\perp, z; t) = \sqrt{N} \phi_\perp(\vec{r}_\perp; \chi(z, t)) \phi_i(z, t), \quad (5)$$

into the transversal and longitudinal functions [41], which in the case of a spin-1 condensate are governed respectively, by

$$\begin{aligned} i\hbar \frac{\partial}{\partial t} \phi_+ &= [h_0 + c_2 N \eta (\rho_+ + \rho_0 - \rho_-)] \phi_+ + c_2 N \eta \phi_0^2 \phi_-^*, \\ i\hbar \frac{\partial}{\partial t} \phi_0 &= [h_0 + c_2 N \eta (\rho_+ + \rho_-)] \phi_0 + 2c_2 N \eta \phi_+ \phi_- \phi_0^*, \\ i\hbar \frac{\partial}{\partial t} \phi_- &= [h_0 + c_2 N \eta (\rho_- + \rho_0 - \rho_+)] \phi_- + c_2 N \eta \phi_0^2 \phi_+^*, \\ \rho \frac{\partial E_\perp}{\partial \chi} + \left(\frac{c_0 N}{2} \rho^2 + \frac{c_2 N}{2} S_2 \right) \frac{\partial \eta}{\partial \chi} &= 0. \end{aligned} \quad (6)$$

In the above, N is the total number of condensed atoms. ϕ_i is the factorized longitudinal envelop function of the quasi-one-dimensional wave function, and it depends only on z and t . ϕ_\perp is the transversal wave function, satisfying $\int d\vec{r}_\perp |\phi_\perp|^2 = 1$, and is assumed to be identical for all three spin components. χ is a variational functional characterizing the width of the transversal wave function. $h_0 = -(\hbar^2/2M)(\partial^2/\partial z^2) + V(z) + E_\perp + c_0 N \eta \rho$ with $V(z) = (M/2)\omega_z^2 z^2$, and E_\perp is the transverse mode energy functional,

$$E_\perp(\chi) = \int d\vec{r}_\perp \phi_\perp^* \left[-\frac{\hbar^2}{2M} \nabla_\perp^2 + \frac{1}{2} M \omega_\perp^2 r_\perp^2 \right] \phi_\perp. \quad (7)$$

$\eta(\chi) = \int d\vec{r}_\perp |\phi_\perp|^4$ is a scaling factor for the nonlinear interaction strength. $\rho(z) = \sum_i |\phi_i|^2$, and S_2 is independent of χ and is shown to be given by

$$\begin{aligned} S_2 &= |\phi_+|^4 + |\phi_-|^4 + 2|\phi_+|^2 |\phi_0|^2 + 2|\phi_-|^2 |\phi_0|^2 \\ &\quad - 2|\phi_+|^2 |\phi_-|^2 + 2\phi_0^{*2} \phi_+ \phi_- + 2\phi_+^* \phi_-^* \phi_0^2. \end{aligned} \quad (8)$$

In obtaining the above relations self-consistently, we have also assumed a weak time and z dependence of the transverse wave function, i.e., $\partial \phi_\perp / \partial t \simeq 0$ and $\nabla^2 \phi_\perp \simeq \nabla_\perp^2 \phi_\perp$.

For a condensate with a large number of atoms, as in most current experiments, the density distribution of the transversal direction approaches the Thomas-Fermi

(TF) limit, $\mu \gg \hbar\omega_{\perp}$, thus we take the TF ansatz for the transverse wave function,

$$\phi_{\perp}(\vec{r}_{\perp}; \chi(z, t)) = \begin{cases} \sqrt{\frac{2}{\pi}} \frac{1}{\chi} \sqrt{1 - \left(\frac{r_{\perp}}{\chi}\right)^2}, & r_{\perp} \leq \chi; \\ 0, & r_{\perp} > \chi. \end{cases}$$

The kinetic energy in the transverse direction is therefore neglected under the TF limit, leading to the transverse mode energy and scaling factor being

$$E_{\perp} = \frac{\hbar\omega_{\perp}}{6} \left(\frac{\chi^2}{a_{\perp}^2} \right),$$

$$\eta = \frac{4}{3\pi\chi^2}.$$

III. SOLITONS IN A TRAPPED SPIN-1 BOSE CONDENSATE

Condensate solitons are within the self-consistent high energy eigenstates of the GP Eq. (3) [42]. Armed with the quasi-1D NPSE approach and the imaginary time propagation method, we perform extensive search for solitonic states. Numerically we first find the ground state, then we propagate the quasi-1D NPSE Eq. (6) in imaginary time domain [43] but subtract out the ground state projection at each time step during evolution,

$$|\phi^{(n)}\rangle \rightarrow |\phi^{(n)}\rangle - \langle\phi^{(0)}|\phi^{(n)}\rangle|\phi^{(0)}\rangle. \quad (9)$$

For the second excited state, we subtract the projections of both the ground state and the first excited state and analogously for higher energy states. The main limitation is the available numerical precision that currently restricts us to be capable of finding only one soliton state which propagates stably. This solitonic state is essentially independent of the choice for the transverse mode as being a fixed Gaussian or a fixed TF ansatz.

An example of the spin-1 soliton found in a trapped ^{87}Rb condensate is illustrated in Fig. 1. The scattering lengths used are $a_0 = 101.8 a_B$ and $a_2 = 100.4 a_B$ with a_B being the Bohr radius [44]. In the subplot Fig. 1(a) we display the spatial distribution of the local spin average that is defined as

$$f_x(z) = \langle F_x \rangle = \sqrt{2} \operatorname{Re}[\phi_0(\phi_0^* + \phi_-^*)]/\rho,$$

$$f_y(z) = \langle F_y \rangle = -\sqrt{2} \operatorname{Im}[\phi_0^*(\phi_+ - \phi_-)]/\rho,$$

$$f_z(z) = \langle F_z \rangle = (|\phi_+|^2 - |\phi_-|^2)/\rho, \quad (10)$$

whose magnitude is given by $f(z) = \sqrt{f_x^2 + f_y^2 + f_z^2}$. We find that the component f_y , which is displayed perpendicular to the plane, remains very close to zero for the soliton, i.e., the local spins stay almost in the x - z plane. We believe the residue small but nonzero value of f_y is due to the numerical precision. Instead of getting rid of these annoying numerical errors, we keep them to study the dynamical stability of the soliton state. Figure 1(a)

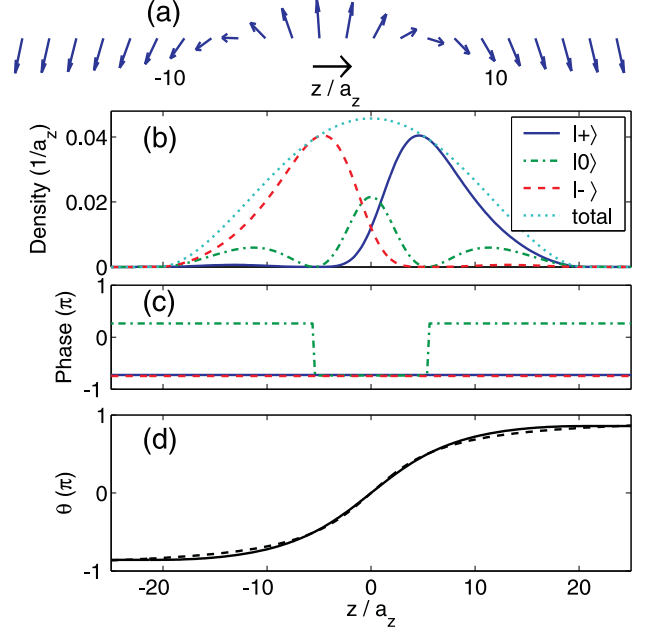


FIG. 1: (Color online) The spatial distribution of the local spin (a), the density (b), and the phase (c) of a soliton state in a trapped spin-1 ^{87}Rb condensate. The trap parameters are $\omega_x = \omega_y = (2\pi)240$ Hz, and $\omega_z = (2\pi)24$ Hz. The total number of atoms in the trap is $N = 10^6$, and the total magnetization ($\mathcal{M} = N_+ - N_-$) is zero. The solid curves in panels (b) and (c) denote the density and the phase for the $|+\rangle$ component, the dash-dotted curves denote the $|0\rangle$ component, the dashed curves denote the $|-\rangle$ component, and the dotted curve in (b) denotes the total density. The solid line in panel (d) shows the local spin angle distribution and the dashed line is for a magnetic kink soliton in homogeneous system.

clearly shows that the local spin rotates nearly a complete revolution, or 2π around the y -axis from one side to the other side of the condensate along the quasi-1D axial direction. It is easy to check that the winding number of this solitonic spin distribution is about one along the y -axis, which shows that the soliton state we find might be related to a quasi-one-dimensional vortex.

We illustrate also the density and the phase distribution in Fig. 1(b) and 1(c). We see a π phase shift in the $|0\rangle$ component near the central region where the density of the $|0\rangle$ component diminishes. Also we notice that the $|+\rangle$ and $|-\rangle$ components are symmetric with respect to the trap center at $z = 0$. The panel (d) shows the angle distribution of local spin (solid line), $\cos\theta = f_z/f$, and a magnetic kink soliton angle distribution (dashed line) given by $\theta = 2 \arctan(z/\xi)$ with the value of $\xi = 5.4a_z$ where the phase of $|0\rangle$ component jumps. The good agreement indicates that the soliton state we find in a trapped spin-1 condensate is closely related to a magnetic kink soliton. The characteristic length ξ is essentially determined by the spin healing length $h/\sqrt{2m|c_2|n}$ [27, 34].

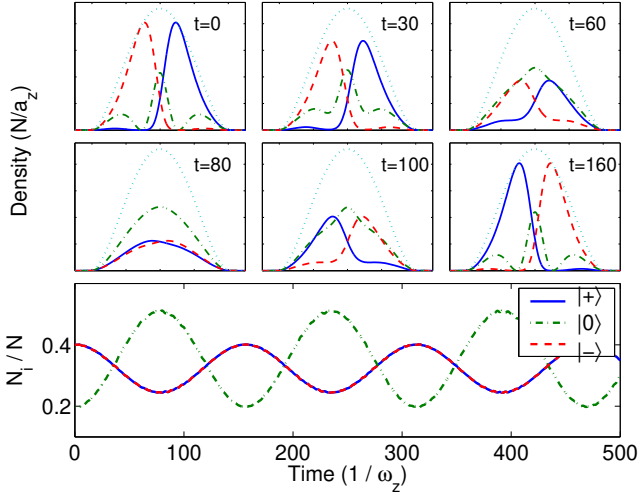


FIG. 2: (Color online) Temporal propagation of the spatial profile of the trapped soliton. The parameters and notations are the same as in Fig. 1. The upper and the middle rows display the density distributions of the soliton at different times. The lower row shows the time dependence of the fractional populations of every spin components.

IV. REAL TIME PROPAGATION OF THE SOLITON IN A TRAP

Starting from the spinor soliton state found above, we can propagate in real time the quasi-1D NPSE in the trap. This allows us to easily check the dynamic stability of the solitonic structure. In addition, we can check several conservative quantities such as the energy, the total number of atoms N , and the total magnetization $\mathcal{M} = N_+ - N_-$ to confirm the accuracy of our numerical integration. During the propagation time $t \in [0, 5000] (1/\omega_z)$, the relative fluctuations of the energy, the number, and the total magnetization are found to be less than 10^{-6} , 10^{-6} , and 10^{-12} , respectively.

We show in Fig. 2 the time dependence of the fractional population for each component, clearly periodic in time. The period is found to be $T \sim 313 (1/\omega_z)$, or equivalent to about 2.1 s in real time unit. For a homogeneous condensate the period goes into infinity which is beyond the scope of this paper and currently unavailable in experiment. For a smaller size condensate, the period decreases. Figure 2 also shows typical density distribution for each component at various times during the first half period. We see the $|+\rangle$ and $|-\rangle$ components tunnel through each other with the assistance of the $|0\rangle$ component and return to their original locations within each period. We note that the $|+\rangle$ and $|-\rangle$ components are immiscible and the tunnelling is generally prohibited without the presence of the $|0\rangle$ component. We do not see such an immiscibility here, since the $|0\rangle$ component provides a cohesion for the $|+\rangle$ and the $|-\rangle$ components. This type of tunnelling process can also be explained in

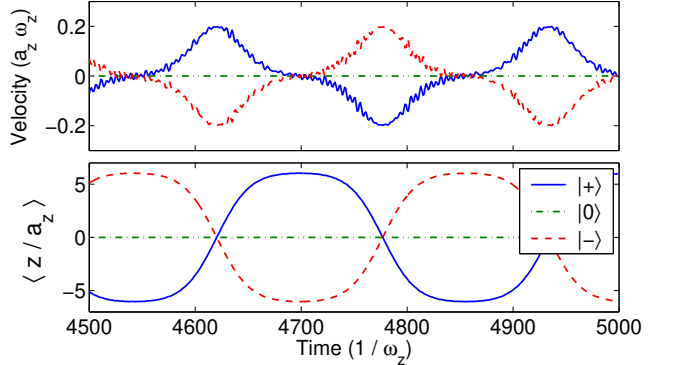


FIG. 3: (Color online) The velocity and the position for the center of mass of each soliton component propagating in a trap. The parameters and notations are the same as in Fig. 1. The motion is periodic, and no noticeable distortion occurs after more than 15 periods or about 33 s.

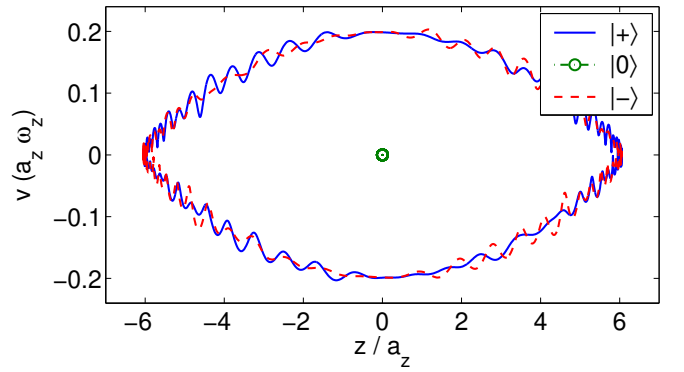


FIG. 4: (Color online) An eye shaped diagram for the phase portrait of the spinor soliton. The parameters and notations are the same as in Fig. 1. Note that the velocity of the $|0\rangle$ component is very close to zero, and there are many small oscillations for the $|+\rangle$ and $|-\rangle$ components.

terms of a mutual precession among the three components as in Ref. [31]. We can actually extract such precession angles for both the $|+\rangle$ and $|-\rangle$ components as equal to π , since they just exchange their positions after the collision, i.e., spin up becomes spin down and vice versa. The interesting feature for a trapped system, distinct from the homogeneous case, is that the tunnelling process repeats itself cyclically upon reflections from the trap boundaries.

Figures 3 and 4 display the position and the velocity of the center of mass (COM) for each component of the solitonic condensate [45]. Complementary to Fig. 2, Fig. 3 shows the oscillations for the last period of our simulation, which lasts from $t = 0$ to $t = 5000 (1/\omega_z)$ with the oscillation period being about $313 (1/\omega_z)$. The velocities of the COM for the $|+\rangle$ and the $|-\rangle$ components exhibit many small oscillation structures while that of the $|0\rangle$

component is always very close to zero. We note from Fig. 3 that the position of the COM for the $|0\rangle$ component is always zero, but the position for the $|+\rangle$ and the $|-\rangle$ components oscillates back and forth periodically and is symmetrically located on the different sides of that of the $|0\rangle$ component. Figure 4 illustrates an eye shaped diagram for the phase portrait of the $|+\rangle$ and the $|-\rangle$ components during the first period. The “eye” opens widely with a clear lid, and the $|0\rangle$ component sits at the center. We note that the fluctuations of the velocities for both the $|+\rangle$ and the $|-\rangle$ components are small near the center of the trap and become enhanced around the turning points of trap boundaries.

Now we comment on the issue of dynamical stability of a ferromagnetically interacting spin-1 Bose condensate. Earlier we studied in Ref. [34], the dynamics of a uniformly distributed spin-1 condensate with ferromagnetic interactions is unstable. While in this study we see little distortion of the wave function after an extended real time propagation even in the presence of initial numerical noise. This clearly indicates the soliton state is dynamically stable. If we compare the soliton state with the final domain structure developed from the homogeneous spin-1 condensate, we see some similarities to their density distributions. These similarities point to a possible connection of the trapped solitonic structure we discuss to the domain structure in the homogeneous case. On a more general term, domain structure can be interpreted as a certain restricted kind of multiple solitons. Previously, Kasamatsu and Tsubota also noticed these similarities between the domains and the solitons in a system of two-component atomic condensates [46].

We note that the oscillation period is about 2 seconds, which is of the order of the experimental lifetime of the condensate [23]. Thus, it remains challenging to observe the spin soliton structure we study here. We also observe that the quantum diffusion time of the spin in the ground state condensate is only a few trap cycles, usually shorter than period of the soliton oscillations [47]. Furthermore, our investigation focuses on excited state solitonic structures where the application of the single spatial mode approximation may become questionable [47]. A more general treatment that potentially addresses these questions seems completely out of reach for the time being. On the other hand, as we reduced to $N = 10^5$, still a large number of trapped atoms, the period of the soliton oscillation reduces due to smaller overlap for the $|\pm\rangle$ components to tunnel through. Thus some aspects of these solitonic structures could become observable with the system parameters being tuned to optimize the intended signals before the condensate disappears.

The detailed local spin evolution of the soliton state is further illustrated in Fig. 5. The magnitude of the local spin $f = \sqrt{f_x^2 + f_y^2 + f_z^2}$ is nearly the same everywhere in space and time. We believe f is exactly the same if a more accurate initial state is used. The spatial distribution of the pointing angles for the local spin, either the azimuthal one φ defined by $\tan \varphi = f_y/f_x$ in Fig. 5(a) or the

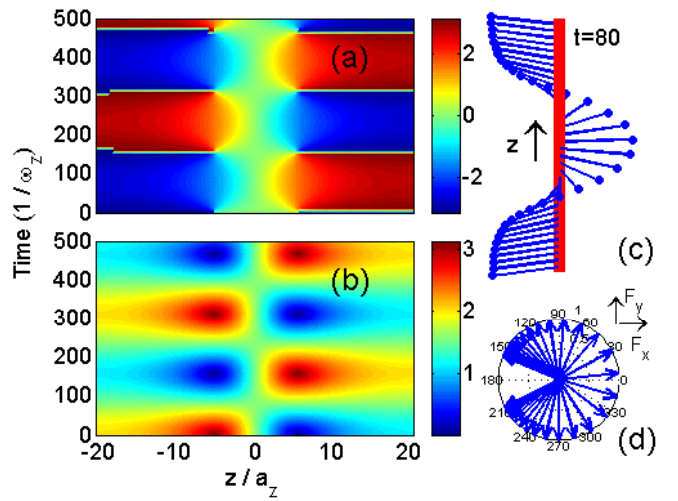


FIG. 5: (Color online) Spatial and temporal distributions of the spin evolution for the spinor condensate soliton. The magnitude of the local spin average is always close to unity due to the ferromagnetic interaction, but the local spin direction evolves with time due to the spin exchange interaction. (a) shows the time dependence of the spatial distribution for the azimuthal spin angle φ and (b) for the polar spin angle θ , (c) shows the typical spatial distribution of the spin average ($t=80$), and (d) shows the projection of the local spin distributions onto the x - y plane.

polar one θ defined by $\cos \theta = f_z/f$ in Fig. 5(b), are strongly periodic. Both angles vary rapidly in the central region and slowly around the boundaries at every moment (the horizontal directions in Fig. 5(a) and (b)). Near the edge of the condensate (the vertical direction), the angle φ essentially remains the same at different times (note $-\pi$ and π represent the same spatial direction), while the polar angle θ changes slightly during each period. θ changes most rapidly with respect to time at about $z = \pm 6a_z$ where the $|+\rangle$ and the $|-\rangle$ components take their highest densities at $t = 0$. In the central region, both angles change moderately with respect to time.

To further clarify the above analysis for the averaged spin directions, we present the 3D spin distribution at time $t = 0$ and $t = 80$ ($1/\omega_z$) in Fig. 1(a) and Fig. 5(c) and (d), respectively. As stated previously, the local spins have nearly zero projections in the y -axis at time $t \simeq 0, T/2, T, \dots$, when they are basically lying in the x - z plane and winding around the y -axis with a winding number of approximately equal to one [Fig. 1(a)]. Similarly, $f_z \simeq 0$ at time $t \simeq T/4, 3T/4, 5T/4, \dots$, when the local spins are lying in the x - y plane but winding around the z -axis with a similar winding number [Fig. 5(c) and (d)]. We find the winding number is a topological quantity that remains conserved during the propagation.

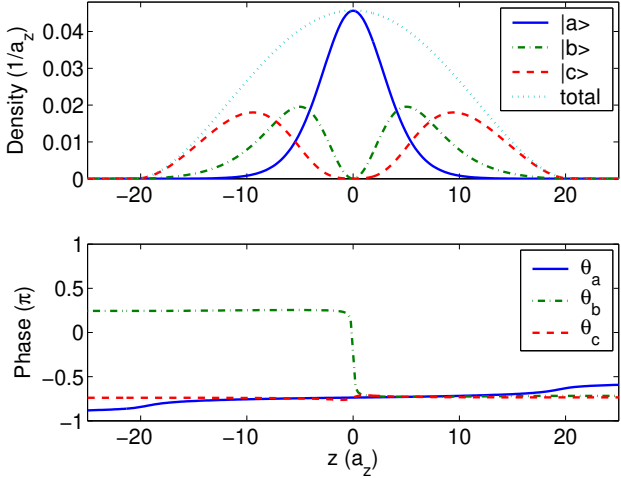


FIG. 6: (Color online) Density and phase distributions of the soliton after the transformation (Eq. 11). The density becomes time independent.

V. STATIONARY SOLITONS IN A ROTATING REFERENCE FRAME

A propagating soliton with a constant speed is actually stationary in a special moving frame. A wonderful story about this is that J. S. Russell once followed the water wave soliton for a couple of miles. Such impressive stability during propagation is also manifested for a soliton in a spin-1 condensate. We find that the density of the soliton becomes time independent with the following canonical transformation,

$$\begin{aligned}\phi_a &= \frac{1}{\sqrt{2}} \left[\frac{1}{\sqrt{2}}(\phi_+ + \phi_-) + \phi_0 \right], \\ \phi_b &= \frac{1}{\sqrt{2}}(\phi_+ - \phi_-), \\ \phi_c &= \frac{1}{\sqrt{2}} \left[\frac{1}{\sqrt{2}}(\phi_+ + \phi_-) - \phi_0 \right].\end{aligned}\quad (11)$$

Figure 6 shows the density and phase distributions of components $|a\rangle$, $|b\rangle$, and $|c\rangle$, which are all time independent after the transformation. The spatial pattern of the phase for each component is also time independent, i.e., θ_a and θ_c are even functions along the axial coordinate with respect to the center of the condensate, and θ_b has a π phase shift at the center of the condensate. We note this density distribution is similar to that of a Mermin-Ho vortex state of Fig. 1 in Ref. [48] again a potential connection of the solitons and the vortex state.

We can choose a new quantization axis z' , different from the axial direction of the condensate, such that ϕ_a , ϕ_b , and ϕ_c correspond to the wave functions of the $|+\rangle$, $|0\rangle$, and $|-\rangle$ components in the new coordinate system. We then find the spatial distribution of $f_{z'} = |\phi_a|^2 - |\phi_c|^2$ is time independent (Fig. 6), and the $f_{x'}$ and $f_{y'}$ rotates with a constant angular velocity around the z' axis as

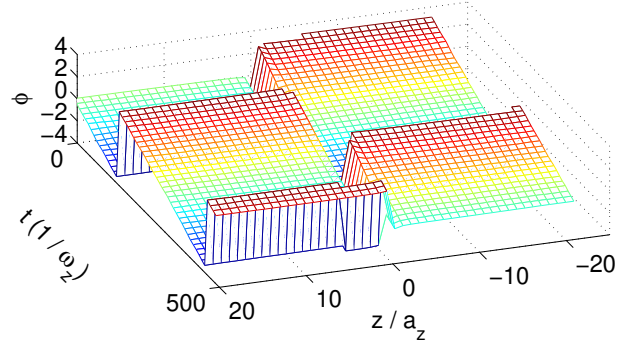


FIG. 7: (Color online) Azimuthal angle of the soliton after the transformation. The spatial pattern of the azimuthal angle is time independent in a rotating reference frame.

shown in Fig. 7. If we go further into the rotating frame defined by

$$\begin{aligned}\hat{x}'' &= \hat{x}' \cos \Omega t + \hat{y}' \sin \Omega t, \\ \hat{y}'' &= -\hat{x}' \sin \Omega t + \hat{y}' \cos \Omega t, \\ \hat{z}'' &= \hat{z}',\end{aligned}\quad (12)$$

where $\Omega = 2\pi/T$, we find the spatial distribution of the spin of the condensate, which is similar to Fig. 1(a), is completely time independent. Thus we show again in the rotating frame (the double primed one) that the appropriate winding number is time independent and remains conserved with change of the reference frame as we confirm previously at the end of the Sec. IV.

Further examination shows that the unitary transformation matrix of Eq. (11) is easily decomposed into spin rotations

$$\begin{aligned}U &= \begin{pmatrix} \frac{1}{2} & \frac{1}{\sqrt{2}} & \frac{1}{2} \\ \frac{1}{\sqrt{2}} & 0 & -\frac{1}{\sqrt{2}} \\ \frac{1}{2} & -\frac{1}{\sqrt{2}} & \frac{1}{2} \end{pmatrix} \\ &= \exp(i\pi) \exp(-iF_y \cdot \frac{\pi}{2}) \exp(-iF_z \cdot \pi).\end{aligned}\quad (13)$$

The new coordinate (x', y', z') after the rotation corresponds to the original $(z, -y, x)$. Thus $f_{x'} = f_z$, $f_{y'} = -f_y$, and $f_{z'} = f_x$. We have checked and confirmed in the original coordinate that f_x is indeed time-independent, i.e., $f_{z'}$ does not change with time (see Fig. 6). We have also found that the time dependence of $\tan^{-1}(-f_y/f_z) = \tan^{-1}(f_{y'}/f_{x'}) = \phi$ is essentially linear as in Fig. 7. Thus we reach the following simplified picture as Fig. 8 in the original coordinate with the given initial conditions as shown in Fig. 1(a): local spins rotate around the x -axis with the same angular frequency $2\pi/T$. This rotation is constrained so that the x -component of the local spin instead of the usual z -component is conserved in the discussed soliton state. An amazing aspect of this local spin processing dynamics is that the equivalent gyro-frequency is independent of space.

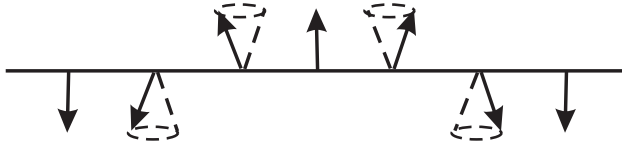


FIG. 8: Schematic diagram of the dynamics of local spins in the new coordinate system.

VI. CONCLUSION

In conclusion, we search numerically for a collectively excited, or a soliton state in a trapped spin-1 ^{87}Rb condensate with ferromagnetic interactions by employing the quasi-one-dimensional nonpolynomial Schrödinger equation (NPSE). We investigate the dynamics of the density, the center of mass motion, and the local spin distribution of the solitonic state we find based on a real time propagation of the NPSE inside the trapped environment. The tunnelling process of the $|\rangle$ and the $|\langle$ components with the assistance of the $|0\rangle$ component is explained as mutual precessions among the different components.

We further show that the soliton state is dynamically stable and is related to the domain structure observed recently in spin-1 ^{87}Rb condensates [27, 34]. By transforming to a rotating reference frame, we demonstrate that the time-dependent dynamics of the local spin of the soliton state become time-independent. In all of the reported numerical simulations we use $N = 10^6$ atoms (although unreported simulations were also performed for $N = 10^5$ as further checks). Within the mean field theory we find that the results are basically the same except that the period becomes shorter for smaller N due to the reduced overlapped region for the $|\pm\rangle$ components to tunnel through.

VII. ACKNOWLEDGEMENT

W. Zhang is indebted to Dr. D. L. Zhou for many stimulating discussions, and he is also grateful to Dr. J. Ieda for providing more recent references [31]. This work is supported by NSF and NASA. O.E.M. acknowledges support from a TUBA-GEBIP Award.

[1] G. P. Agrawal, *Nonlinear fiber optics*, (Academic Press, Boston, 1989).

[2] P. G. Drazin and R. S. Johnson, *Solitons: an introduction*, (Cambridge University Press, 1989).

[3] K. E. Lonngren, *Plasma Physics* **25**, 943 (1983).

[4] M. Wu, B. A. Kalinkos, and C. E. Patton, *Phys. Rev. Lett.* **93**, 157207 (2004).

[5] H. Leblond and V. Veerakumar, *Phys. Rev. B* **70**, 134413 (2004).

[6] K. E. Strecker, G. B. Partridge, A. G. Truscott, and R. G. Hulet, *Nature (London)* **417**, 150 (2002).

[7] M. H. Anderson, J. R. Ensher, M. R. Matthews, C. E. Wieman, and E. A. Cornell, *Science* **269**, 198 (1995).

[8] K. B. Davis, M.-O. Mewes, M. R. Andrews, N. J. van Druten, D. S. Durfee, D. M. Stamper-Kurn, and W. Ketterle, *Phys. Rev. Lett.* **75**, 3969 (1995).

[9] C. C. Bradley, C. A. Sackett, J. J. Tollett, and R. G. Hulet, *Phys. Rev. Lett.* **75**, 1687 (1995); Erratum: *ibid* **79**, 1170 (1997).

[10] C. J. Pethick and H. Smith, *Bose-Einstein condensation in dilute gases*, (Cambridge University Press, 2002).

[11] L. Pitaevskii and S. Stringari, *Bose-Einstein condensation*, (Clarendon Press, Oxford, 2003).

[12] F. Dalfovo, S. Giorgini, L. P. Pitaevskii, and S. Stringari, *Rev. Mod. Phys.* **71**, 463 (1999).

[13] S. L. Cornish, N. R. Claussen, J. L. Roberts, E. A. Cornell, and C. E. Wieman, *Phys. Rev. Lett.* **85**, 1795 (2000).

[14] S. Burger, K. Bongs, S. Dettmer, W. Ertmer, K. Sengstock, A. Sanpera, G. V. Shlyapnikov, and M. Lewenstein, *Phys. Rev. Lett.* **83**, 5198 (1999).

[15] J. Denschlag, J. E. Simsarian, D. L. Feder, C. W. Clark, L. A. Collins, J. Cubizolles, L. Deng, E. W. Hagley, K. Helmerson, W. P. Reinhardt, S. L. Rolston, B. I. Schneidler, and W. D. Phillips, *Science* **287**, 97 (2000).

[16] J. Babarro, M. J. Paz-Alonso, H. Michinel, J. R. Salgueiro, and D. N. Olivier, *Phys. Rev. A* **71**, 043608 (2005).

[17] V. M. Pérez-García and J. B. Beitia, *Phys. Rev. A* **72**, 033620 (2005).

[18] S. Coen and M. Haelterman, *Phys. Rev. Lett.* **87**, 140401 (2001).

[19] J. Stenger, S. Inouye, D. M. Stamper-Kurn, H. -J. Miesner, A. P. Chikkatur, and W. Ketterle, *Nature* **396**, 345 (1998).

[20] D. M. Stamper-Kurn, M. R. Andrews, A. P. Chikkatur, S. Inouye, H. -J. Miesner, J. Stenger, and W. Ketterle, *Phys. Rev. Lett.* **80**, 2027 (1998).

[21] D. M. Stamper-Kurn and W. Ketterle, *Spinor condensates and light scattering from Bose-Einstein condensates*, in the Proceedings of Les Houches 1999 Summer School, Session LXXII, (New York: Springer-Verlag) (1999).

[22] M. D. Barrett, J. A. Sauer and M. S. Chapman, *Phys. Rev. Lett.* **87**, 010404 (2001).

[23] M.-S. Chang, C. D. Hamley, M. D. Barrett, J. A. Sauer, K. M. Fortier, W. Zhang, L. You, and M. S. Chapman, *Phys. Rev. Lett.* **92**, 140403 (2004).

[24] H. Schmaljohann, M. Erhard, J. Kronjäger, M. Kottke, S. van Staa, L. Cacciapuoti, J. J. Arlt, K. Bongs, and K. Sengstock, *Phys. Rev. Lett.* **92**, 040402 (2004).

[25] T. Kuwamoto, K. Araki, T. Eno, and T. Hirano, *Phys. Rev. A* **69**, 063604 (2004).

[26] J. M. Higbie, L. E. Sadler, S. Inouye, A. P. Chikkatur, S. R. Leslie, K. L. Moore, V. Savalli, and D. M. Stamper-Kurn, *Phys. Rev. Lett.* **95**, 050401 (2005).

[27] M.-S. Chang, Q. Qin, W. Zhang, L. You, and M. S. Chapman, *Nature Phys.* **1**, 111 (2005).

- [28] T. -L. Ho, Phys. Rev. Lett. **81**, 742 (1998).
- [29] T. Ohmi and K. Machida, J. Phys. Soc. Jpn. **67**, 1822 (1998)
- [30] C. K. Law, H. Pu and N. P. Bigelow, Phys. Rev. Lett. **81**, 5257 (1998).
- [31] J. Ieda, T. Miyakawa, and M. Wadati, Phys. Rev. Lett. **93**, 194102 (2004); J. Ieda, T. Miyakawa, and M. Wadati, J. Phys. Soc. Jpn. **73**, 2996 (2004); M. Wadati and N. Tsuchida, J. Phys. Soc. Jpn. **75**, 014301 (2006); J. Ieda, M. Uchiyama, and M. Wadati, eprint nlin.SI/0603010; M. Uchiyama, J. Ieda, and M. Wadati, J. Phys. Soc. Jpn **75**, 064002 (2006).
- [32] Z. Xie, W. Zhang, S. T. Chui, and W. M. Liu, Phys. Rev. A **69**, 053609 (2004).
- [33] Z. D. Li, P. B. He, L. Li, J. Q. Liang, and W. M. Liu, Phys. Rev. A **71**, 053611 (2005).
- [34] W. Zhang, D. L. Zhou, M.-S. Chang, M. S. Chapman, and L. You, Phys. Rev. Lett. **95**, 180403 (2005).
- [35] H. Saito and M. Ueda, Phys. Rev. A **72**, 023610 (2005).
- [36] A. D. Jackson, G. M. Kavoulakis, and C. J. Pethick, Phys. Rev. A **58**, 2417 (1998).
- [37] L. Salasnich, A. Parola, and L. Reatto, Phys. Rev. A **65**, 043614 (2002).
- [38] L. Salasnich, Phys. Rev. A **70**, 053617 (2004).
- [39] M. L. Chiofalo and M. P. Tosi, Phys. Lett. A **268**, 406 (2000).
- [40] F. Gerbier, Europhys. Lett. **66**, 771 (2004).
- [41] W. Zhang and L. You, Phys. Rev. A **71**, 025603 (2005).
- [42] D. L. Feder, M. S. Pindzola, L. A. Collins, B. I. Schneider, and C. W. Clark, Phys. Rev. A **62**, 053606 (2000).
- [43] S. Yi, Ö. E. Müstecaplıoğlu, C. P. Sun, and L. You, Phys. Rev. A **66**, 011601(R) (2002); W. Zhang, S. Yi, and L. You, Phys. Rev. A **70**, 043611 (2004).
- [44] E. G. M. van Kempen, S. J. J. M. F. Kokkelmans, D. J. Heinzen, and B. J. Verhaar, Phys. Rev. Lett. **88**, 093201 (2002).
- [45] G. Huang, M. G. Velarde, and V. A. Makarov, Phys. Rev. A **64**, 013617 (2001).
- [46] K. Kasamatsu and M. Tsubota, Phys. Rev. Lett. **93**, 100402 (2004).
- [47] S. Yi, Ö. E. Müstecaplıoğlu, and L. You, Phys. Rev. Lett. **90**, 140404 (2003); *ibid.*, Phys. Rev. A **68**, 013613 (2003).
- [48] T. Mizushima, K. Machida, and T. Kita, Phys. Rev. Lett. **89**, 030401 (2002).